scientific reports

OPEN

Darcy resistance flow of Sutterby nanofluid with microorganisms with applications of nano-biofuel cells

Abdulmajeed Aldabesh[1], A. Haredy[2], Kamel Al-Khaled[3], Sami Ullah Khan[4] & Iskander Tlili[5]✉

The objective of current research is to endorse the thermal aspect of Sutterby nanofluid containing the microorganisms due the stretched cylinder. The features of nonlinear thermal radiation, Darcy resistance and activation energy are also incorporated to inspect the thermal prospective. The problem is further extended with implementation of modified Fourier and Fick's theories. The results are presented for the stretched cylinder and also for stationary plate. The numerical formulation for the problem is presented by following the shooting technique. The comparative numerical is performed to verify the computed simulations. The results convey that the presence of Darcy resistance parameter enhanced the velocity more effectively for stretched cylinder. A reduction in velocity due to Sutterby fluid parameter and buoyancy ratio parameter has been observed. Moreover, the temperature profile enhanced with larger sponginess parameter more effectively for stretching cylinder.

Nomenclature

T_w^*	Surface temperature
N_w^*	Surface microorganisms density
C_∞^*	Free stream concentration
(u_1, w_1)	Velocity components
c_p	Specific heat
ρ_m	The microorganisms density
C	Concentration of nanoparticles
D_B^*	Brownian motion coefficient
D_m	Microorganisms diffusion coefficients
n	Fitted rate constant,
b	Stand for chemotaxis constant
λ_a	Heat relaxation time
N	Density of microorganisms
M	Hartmann number
β	Curvature parameter
α_1	Sutterby nanofluid parameter
α_2	Darcy resistance parameter
λ_T	Thermal relaxation parameter
Nt	Thermophoresis parameter
Rd	Thermal radiation parameter
σ	Chemical reaction parameter
Lb	Bioconvection Lewis number
γ	Biot number, respectively

[1]Department of Mechanical Engineering, Faculty of Engineering, Albaha University, Al Bahah 65527, Saudi Arabia. [2]Department of Architecture, Faculty of Engineering, Albaha University, Al Bahah 65527, Saudi Arabia. [3]Department of Mathematics and Statistics, Jordan University of Science and Technology, P.O. Box 3030, Irbid 22110, Jordan. [4]Department of Mathematics, COMSATS University Islamabad, Sahiwal 57000, Pakistan. [5]Physics Department, College of Science Al-Zulfi, Majmaah University, Al-Majmaah 11952, Saudi Arabia. ✉email: l.tlili@mu.edu.sa

Nb	Brownian motion parameter
δ_0	Temperature difference parameter
j_m	For local mass flux
Re	Reynold number
C_w^*	Surface concentration
T_∞^*	Surface temperature
N_∞^*	Free stream microorganisms density
ρ_f	Fluid density
α^2	Consistency index
ρ_p	Density of nanoparticles
T	Temperature of nanoparticles
D_T^*	Thermophoresis diffusion coefficient
Kr	Chemical reaction constant
m^*	Flow comportment index
E	Coefficient of activation energy
λ_b	Mass relaxation time
W_e	Cell swimming speed
S^*	Mixed convection parameter
A_1	Buoyancy ratio parameter
A_2	Bioconvection Rayleigh number
α	Sponginess parameter
Pr	Prandtl number
Le	Lewis number
θ_w	Temperature ratio parameter
E	Activation energy parameter
Pe	Peclet number
ϖ	Microorganisms difference parameter
λ_C	Mass relaxation parameter
q_m	Local heat flux
j_n	Microorganisms flux

In today's growing world of technology, most engineers, scientists and researchers are focused on the analysis of nanoliquid due to their physical applications in the field of applied sciences. Nanofluids are known to be the accumulation of micro-shape solid objects in the convectional fluid. The accumulation of micro-shaped solid objects in the convection fluid is considered to be nanofluids. The enhancement in the heating capacity is necessary in different range of industrial and engineering mechanisms. The availability of increasing heat source is necessary to improve the optimal growth of industrial products. The communication and growing research in nanofluids predict novel thermal applications of such particle in the energy sector, power plants, chemical processes, engineering devices, thermal mechanisms etc. Choi[1] explored the novel thermal aspect of nanofluids in primary research via experimental support. Alharbi[2] studied flow of hybrid nanofluids with heat energy impacts. Uddinet al.[3] scrutinized the radiative slip impact in nanofluid. Hassan et al.[4] focused the thermal availably of hybrid nanofluid by assuming the shear thinning as a base liquid. Tlili et al.[5] premeditated the thermal flow of Oldroyd-B nanofluid with isotropic slip impact. Khan et al.[6] analyzed Darcy-Forchheimer flow in hybrid nanofluid. Haq et al.[7] focused the improve thermal properties of nanofluid with suspension of Casson liquid. Xia et al.[8] addressed the natural convective optimized analysis for Eyring-Powell nanofluid subject to microorganisms. The cross nanofluid flow with entropy generation assessment was utilized by Haq et al.[9]. In another reports, Haq et al.[10] inspected the bioconvection applications for the nanofluid flow with controlled optimized phenomenon. Hussain et al.[11] observed the carbon nanotube thermal outcomes with fluctuation of dynamic viscosity. The melting applications for hybrid nanofluid in addition of variable viscosity has been intended by Hussain et al.[12]. The analysis of Hussain et al.[13] reports the improved heat transfer analysis for Jeffrey material with external heat source. Some more recent research on nanofluids is referred to refs.[14–17].

The Sutterby nanofluid study is another topic of interest to enhance the thermal features of base fluids. Mir et al.[18] addressed the relative improvement of heat transportation phenomenon by endorsing the Sutterby nanofluid in base liquid. The thermal research via interaction of Sutterby nanofluid with progressive thermal change was explored by Nawaz et al.[19]. Bilal et al.[20] observed the role of magnetic force for Sutterby nanofluid flow. The influence of thermal radiation and the inclined magnetic field on the Sutterby fluid by focusing on the Cattaneo-Christov heat flux structure is examined by Sabir et al.[21]. Song et al.[22] performed the Marangoni convection analysis for Sutterby nanofluid with melting and solutal constraints. Abbasi et al.[23] endorsed the Sutterby nanoparticles properties in trapped channel.

The self-induced motile micro-organisms can increase the density of ordinary fluids in specific direction and, as a response a bioconvection phenomenon has evolved. Such nanoparticles motion is independent of microorganism movement and therefore the collective functionality of bioconvection and nanofluids seems to also be vital for microfluidics devices. Waqas et al.[24] reported the bio-convective model for generalized viscoelastic nanofluid by performing the numerical simulations. Aziz et al.[25] tackled a bidirectional bioconvection thermal nanofluid problem subject to accelerating space. Khan et al.[26] discovered the theoretical continuation for couple stress nanofluid with consequences of activation energy and bioconvection phenomenon. Tong et al.[27] explored the suspension of microorganisms subject to slip implementation for nanofluid. Li et al.[28] reported the

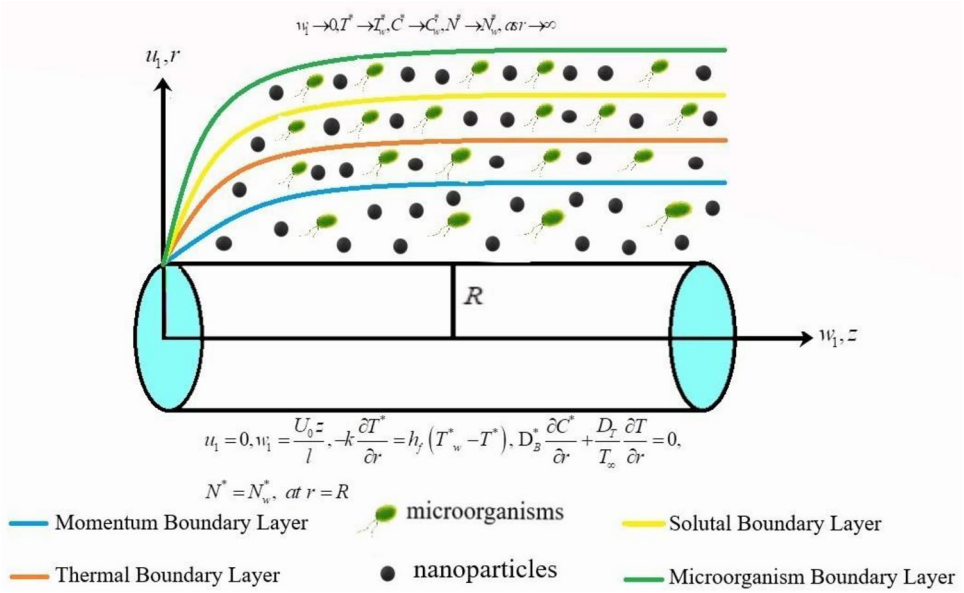

Figure 1. Physical view of flow.

bio-convection applications for modified second grade fluid. Alwatban et al.[29] expressed the physical onset of bioconvection phenomenon regarding the nanofluid flow.

Although a lot of research have been performed on the nanofluids, however, the thermal applications of Sutterby nanofluid subject to the bioconvection phenomenon with diverse flow features has not been performed yet. One this end, this research presents the thermal flow of Sutterby nanofluid containing the microorganisms due to moving cylinder. The navel aspects of this model are:

- The Darcy resistance flow of radiated Sutterby nanofluid with microorganisms due moving cylinder is presented.
- The Fourier and Fick's modified expressions are used for examining the heat and mass transfer phenomenon.
- The novel thermal features like nonlinear thermal radiation and activation energy are also incorporated.
- The convective boundary conditions are utilized with motivations of enhancing the thermal transport of Sutterby nanofluid.
- The shooting technique for the formulated boundary value problem is implemented for obtained numerical simulations.
- The obtained simulations may present novel significances in bio-fuels, enzymes, thermal processes, energy systems, heat transfer devices etc.

Flow model

The thermal transport of Sutterby nanofluid with consideration of suspension of microorganisms is taken into consideration. The stretched cylinder is assumed to originate the laminar flow. The velocity of moving cylinder is attributed to be $U_w(z) = U_0 z/l$. The normal aspect of magnetic force is also utilized[30]. The consequence of activation energy for solutal transport is discussed. A physical schematic of flow model is depicted in Fig. 1. Moreover T_w^*, C_w^* and N_w^* signifies wall surface temperature, concentration and microorganisms respectively. Here ambient temperature, concentration and microorganisms are symbolized by T_∞^*, C_∞^* and N_∞^* correspondingly.

Under the above postulations, the leading governing boundary layer equations of flow are given as follows[18–20]:

$$\frac{\partial u_1}{\partial r} + \frac{u_1}{r} + \frac{\partial w_1}{\partial z} = 0, \tag{1}$$

$$\begin{aligned} u_1\frac{\partial w_1}{\partial r} + w_1\frac{\partial w_1}{\partial z} &= \frac{\nu_a}{2}\frac{\partial^2 w_1}{\partial r^2} + \frac{\nu_a}{2r}\frac{\partial w_1}{\partial r} - \frac{\nu_a m^* \alpha^2}{4}\left(\frac{\partial w_1}{\partial r}\right)^2\frac{\partial^2 w_1}{\partial r^2} + \frac{\sigma B_o^2}{\rho_f}w_1 \\ &+ \frac{R_z}{\rho_f} + \frac{1}{\rho_f}\left[\begin{array}{l}\left(1-C_f\right)\rho_f\beta^{**}g*(T-T_\infty) - \left(\rho_p - \rho_f\right)g^*(C-C_\infty) \\ -(N-N_\infty)g^*\gamma\left(\rho_m - \rho_f\right)\end{array}\right], \end{aligned} \tag{2}$$

$$\left[u_1\frac{\partial T^*}{\partial r}+w_1\frac{\partial T^*}{\partial z}\right]+\lambda_a C_H^*=\frac{K^*}{(\rho_f C_p)}\left[\frac{\partial^2 T^*}{\partial r^2}+\frac{1}{r}\frac{\partial T^*}{\partial r}\right]$$
$$+\frac{\tau}{(\rho_f C_p)}\left[D_B^*\frac{\partial C^*}{\partial r}\frac{\partial T^*}{\partial r}+\frac{D_{T^*}^*}{D_B^*}\left(\frac{\partial T^*}{\partial r}\right)^2\right]+\frac{1}{(\rho c)_f}\frac{1}{r}\frac{\partial}{\partial r}\left(r\frac{16\sigma^*}{3k^*}T^{*3}\frac{\partial T^*}{\partial r}\right), \tag{3}$$

Here,

$$C_H^*=u_1^2\frac{\partial^2 T^*}{\partial r^2}+w_1^2\frac{\partial^2 T^*}{\partial z^2}+2u_1w_1\frac{\partial^2 T^*}{\partial r\partial z}+u_1\frac{\partial u_1}{\partial r}\frac{\partial T^*}{\partial z}+u_1\frac{\partial w_1}{\partial r}\frac{\partial T^*}{\partial z}+w_1\frac{\partial u_1}{\partial z}\frac{\partial T^*}{\partial r}$$
$$+w_1\frac{\partial w_1}{\partial r}\frac{\partial T^*}{\partial z} \tag{4}$$

$$\left[u_1\frac{\partial C^*}{\partial r}+w_1\frac{\partial C^*}{\partial z}\right]+\lambda_a C_H^*=D_B^*\left[\frac{\partial^2 C^*}{\partial r^2}+\frac{1}{r}\frac{\partial C^*}{\partial r}\right]+\frac{D_{T^*}^*}{D_B^*}\left[\frac{\partial^2 T^*}{\partial r^2}+\frac{1}{r}\frac{\partial T^*}{\partial r}\right]$$
$$-Kr^2\left(C^*-C_\infty^*\right)\left(\frac{T^*}{T_\infty^*}\right)^n\exp\left(\frac{-E_a}{kT^*}\right), \tag{5}$$

where

$$C_H^*=u_1^2\frac{\partial^2 C^*}{\partial r^2}+w_1^2\frac{\partial^2 C^*}{\partial z^2}+2u_1w_1\frac{\partial^2 C^*}{\partial r\partial z}+u_1\frac{\partial u_1}{\partial r}\frac{\partial C^*}{\partial z}+u_1\frac{\partial w_1}{\partial r}\frac{\partial C^*}{\partial z}$$
$$+w_1\frac{\partial u_1}{\partial z}\frac{\partial C^*}{\partial r}+w_1\frac{\partial w_1}{\partial r}\frac{\partial C^*}{\partial z} \tag{6}$$

$$u_1\frac{\partial N^*}{\partial r}+w_1\frac{\partial N^*}{\partial z}+\left[\frac{\partial}{\partial r}\left(N^*\frac{\partial C^*}{\partial r}\right)\right]\frac{bW_c}{\left(C_w^*-C_\infty^*\right)}=D_m\frac{\partial}{\partial r}\left(\frac{\partial N^*}{\partial r}\right), \tag{7}$$

with boundary conditions:

$$u_1=0, w_1=\frac{U_0 z}{l}, -k\frac{\partial T^*}{\partial r}=h_f\left(T_w^*-T^*\right),\ D_B^*\frac{\partial C^*}{\partial r}+\frac{D_T}{T_\infty}\frac{\partial T}{\partial r}=0, N^*=N_w^*,\ \ at\ r=R,$$
$$w_1\to 0, T^*\to T_w^*, C^*\to C_w^*, N^*\to N_w^*,\ \ as\ r\to\infty \tag{8}$$

In the above Eq. (2) Darcy resistance is defined as[31]:

$$R=-\frac{\mu}{2k^*}\left[\frac{\sinh^{-1}(\alpha\gamma)}{\alpha\gamma}\right]^m\mathbf{V}, \tag{9}$$

Introducing the following suitable similarities variables[18–20]:

$$\zeta=\sqrt{\frac{U_0}{\nu_a l}}\left(\frac{r^2-R^2}{2R}\right),\ u_1=\sqrt{\frac{\nu_a U_0}{l}}\frac{R}{r}f(\zeta),\ w_1=-\frac{U_0 z}{l}f'(\zeta),$$
$$\theta(\zeta)=\frac{T^*-T_\infty^*}{T_w^*-T_\infty^*},\ \phi(\zeta)=\frac{C^*-C_\infty^*}{C_w^*-C_\infty^*},\ \chi(\zeta)=\frac{N^*-N_\infty^*}{N_w^*-N_\infty^*}. \tag{10}$$

After introducing the above appropriate transformation (10) in governing PDE's, we acquire

$$(1+2\beta\zeta)f'''+2ff''-2\left(f'\right)^2-\frac{\alpha_1}{2}(1+2\beta\zeta)\left(f''\right)^2f'''+\beta f''-\left(M+\frac{\alpha}{2}\right)f'+\frac{1}{12}\alpha_2 f'f''$$
$$+S^*[\theta-A_1\phi-A_2\chi]=0, \tag{11}$$

$$\left[\left\{1+Rd(1+(\theta_w-1)\theta)^3\right\}(1+2\beta\zeta)\theta'\right]\theta''+2\beta\theta'+Prf\theta'+Pr(1+2\beta\zeta)\left[Nb\theta'\phi'+Nt\left(\theta'\right)^2\right]$$
$$-Pr\lambda_T\left[ff'\theta'+f^2\theta''\right]=0, \tag{12}$$

$$(1+2\beta\zeta)\phi''+2\beta\phi'+LePrf\phi'+LePr\frac{Nt}{Nb}\left[(1+2\beta\zeta)\theta''+\beta\theta'\right]-LePr\lambda_C\left[ff'\phi'+f^2\phi''\right]$$
$$-Le\,\mathrm{Pr}\,\sigma(1+\delta_0\theta)^n\phi\exp\left(-\frac{E}{1+\delta_0\theta}\right)=0, \tag{13}$$

$$(1+2\beta\zeta)\chi''+2\beta\chi'+Lb\chi' f-Pe\left(\phi''(\chi+\varpi)+\chi'\phi'\right)=0, \tag{14}$$

With

$$\begin{aligned} &f(\zeta)=0, f'(\zeta)=1, \theta'=-\gamma(1-\theta(\zeta)),\\ &Nb\phi'(\zeta)+Nt\theta'(\zeta)\ , \chi'(\zeta)=1 \ \ at\ \zeta=0,\\ &f'\to 0,\ \theta\to 0,\ \phi\to 0,\ \chi\to 0,\ \ as\ \zeta\to\infty \end{aligned} \tag{15}$$

with dimensionless parameter:

$$\begin{aligned} &M=\frac{l\sigma B_0^2}{\rho_f U_0}, S^*=\frac{l^2\beta^{**}g^*\left(1-C_\infty^*\right)\left(T_w^*-T_\infty^*\right)}{zU_0^2}, \beta=\frac{1}{R}\sqrt{\frac{\nu_a l}{U_0}}, A_1=\frac{\left(C_w^*-C_\infty^*\right)\left(\rho_p-\rho_f\right)}{\rho_f\beta^{**}\left(1-C_w^*\right)\left(T_w^*-T_\infty^*\right)},\\ &\alpha_1=\frac{m^*\alpha^2U_0^3z^2}{l^3\nu_a}, A_2=\frac{\gamma^*\left(\rho_m-\rho_f\right)\left(N_w^*-N_\infty^*\right)}{\rho_f\beta^{**}\left(1-C_w^*\right)\left(T_w^*-T_\infty^*\right)}, \alpha_2=\frac{m^*\alpha^2U_0^2z^2}{l^2k^*}, \alpha=\frac{\nu_a l}{k^*U_0}, \lambda_T=\frac{\lambda_a U_0}{l},\\ &Pr=\frac{\nu_a}{\alpha}, Nt=\left(\frac{\tau D_{T^*}^*\left(T_w^*-T_\infty^*\right)}{\nu_a T_\infty^*}\right), Le=\frac{\alpha}{D_B^*}, Rd=\frac{16\sigma^*T_\infty^3}{3kk^*}, \theta_w=\frac{T_w^*}{T_\infty^*}, \sigma=\frac{lKr^2}{U_0}, E=\frac{E_a}{kT_\infty},\\ &Nb=\left(\frac{\tau D_B^*\left(C_w^*-C_\infty^*\right)}{\nu_a}\right), \lambda_C=\frac{\lambda_b U_0}{l}, \delta_0=\frac{T_w^*-T_\infty^*}{T_\infty^*}, Lb=\frac{\nu_a}{D_m}, Pe=\frac{bW_c}{D_m}, \varpi=\frac{N_\infty^*}{N_w^*-N_\infty^*},\\ &\gamma=\frac{h_f}{k}\sqrt{\frac{\nu_a l}{U_0}}. \end{aligned} \tag{16}$$

Physical quantities of interest are

$$Nu_z=\frac{zq_m}{k\left(T_w^*-T_\infty\right)}, Sh_z=\frac{zj_m}{D_B^*\left(C_w^*-C_\infty^*\right)}, Sn_z=\frac{zj_m}{D_m^*\left(N_w^*-N_\infty^*\right)}. \tag{17}$$

q_m the local heat flux, j_m for local mass flux and j_n microorganisms flux, which are addressed as

$$q_m=-k\left(\frac{\partial T}{\partial r}\right)_{r=R}-, j_m=-D_B\left(\frac{\partial C}{\partial r}\right)_{r=R}, j_n=-D_m\left(\frac{\partial N}{\partial r}\right)_{r=R} \tag{18}$$

In the dimensionless forms are

$$Nu_z\mathrm{Re}_z^{-\frac{1}{2}}=-\left(1+\frac{4}{3}R_d(1+(\theta_w-1)\theta(0))\right)^3\theta'(0), Sh_z\mathrm{Re}_z^{-\frac{1}{2}}=-\phi'(0), Sn_z\mathrm{Re}_z^{-\frac{1}{2}}=-\chi'(0) \tag{19}$$

Here the local Reynolds number is symbolized by $\mathrm{Re}_z=\frac{U_0 z}{\nu_a}$.

Numerical procedure

The coupled governing odrinary differential Eqs. (11–14) with boundary restrictions (15) is higly nonlinear in nature. The numerical solutions of these system is very diffecullt. There for obtain numerical solutions of model we employ shooting technique via Matlab tool bvp4c. initially, the higher-order ODE's are converted into first order system, by implementing following procedure

$$\left.\begin{aligned} &f=t_1, f'=t_2, f''=t_3, f'''=t_3',, \theta=t_4, \theta'=t_5, \theta''=t_5',\phi=t_6,\\ &\phi'=t_7, \phi''=t_7', \chi=t_8, \chi'=t_9, \chi''=t_9' \end{aligned}\right\}, \tag{20}$$

$$t_3'=\frac{-2tt_3+2t_2^2-\beta t_3+\left(M+\frac{\alpha}{2}\right)t_2-\frac{1}{12}\alpha_2 t_2 t_3-S^*[t_4-A_1t_6-A_2t_8]}{\left(1-\frac{\alpha_1}{2}t_3^2\right)(1+2\beta\zeta)}, \tag{21}$$

$$t_5'=\frac{-2\beta t_5-Pr\,tt_5-Pr(1+2\beta\zeta)\left[Nbt_5t_7+Nt\,t_5^2\right]+Pr\lambda_T[tt_2t_5]}{\left(\left[\left\{1+Rd(1+(\theta_w-1)t_4)^3\right\}(1+2\beta\zeta)t_5\right]-Pr\lambda_T t^2\right)}, \tag{22}$$

$$t_7'=\frac{\begin{aligned}&-2\beta t_7-LePrtt_7-LePr\frac{Nt}{Nb}\left[(1+2\beta\zeta)t_5'+\beta t_5\right]+LePr\lambda_C[tt_1t_7]\\&+LePr\sigma(1+\delta_0t_4)^n t_6\exp\left(-\frac{E}{1+\delta_0t_4}\right)\end{aligned}}{\left((1+2\beta\zeta)-LePr\lambda_C t^2\right)}, \tag{23}$$

$$t_9'=\frac{-2\beta t_9-Lbt_9t+Pe\left(t_7'(t_8+\varpi)+t_9t_7\right)}{(1+2\beta\zeta)}, \tag{24}$$

M	Fathizadeh et al.[32]			Fang et al.[33]	Present results
	HPM	MHPM	Exact solution		
0	1	1	1	1	1.0000
1.0	− 1.4142	− 1.4142	− 1.4142	− 1.4142	− 1.4145

Table 1. The comparative analysis when $\beta = S^* = A_1 = A_2 = \alpha = 0$.

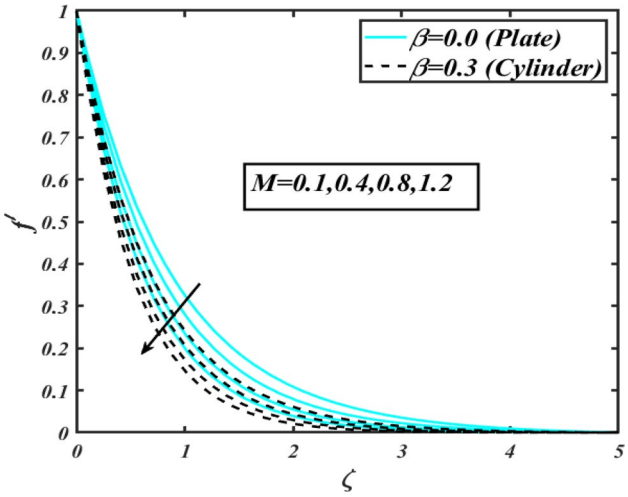

Figure 2. Profile of f' for M.

$$\begin{aligned} &t(\zeta) = 0, t_2(\zeta) = 1, t_5 = -\gamma(1 - t_4(\zeta)), \\ &Nbt_7(\zeta) + Nt\, t_5(\zeta)\ ,\ t_9(\zeta) = 1 \ \ at\ \zeta = 0, \\ &t_2 \to 0,\ \ t_4 \to 0,\ t_6 \to 0, t_8 \to 0,\ \ as\ \zeta \to \infty \end{aligned} \tag{25}$$

Validation of results

The solution verification and validity has been checked in Table 1 with comparison the numerical with investigation of Fathizadeh et al.[32] and Fang et al.[33]. A fine accuracy of obtained results is noted with these studies.

Results and discussion

This section communicates the physical aspect of Sutterby nanofluid in view of flow parameters. The comparative analysis is performed for flow due to plate ($\beta = 0.0$) and cylinder ($\beta = 0.3$). Figure 2 is drawn to estimate the consequence of Hartmann number M on flow velocity f'. The interaction of magnetic force reports a declining change in velocity due to presence of Lorentz force. Moreover, the declining change in velocity is more progressive for plate as compared to stretched cylinder. Figure 3 characterizes the impact of Sutterby fluid parameter α_1 on velocity f'. The velocity f' dwindles for increasing change in Sutterby fluid parameter α_1. The outcomes of f' against Darcy resistance parameter α_2 is delineated via Fig. 4. An increasing change in velocity enhanced the f' for Darcy resistance parameter α_2. Figure 5 is portrayed to understand the impact of buoyancy ratio parameter A_1 on f' It is analyzed that f' reduces for increasing variation of A_1 for both plate ($\beta = 0.0$) and stretched cylinder ($\beta = 0.3$). Physically, the buoyancy forces play novel contribution to reduce the velocity rate effectively. Figure 6 is plotted to investigate the insight of bioconvection Rayleigh factor A_2 on f'. The velocity field f' exaggerates for larger bioconvection Rayleigh number A_2. Figure 7 is illustrating the deviation of mixed convection parameter S^* on f' for both plate and cylinder. The depicted change in f' show an increasing fluctuation by raise in estimation of mixed convection parameter S^*. Physically, the mixed convection constant explores the ratio between buoyancy to viscous force. The increasing contributions of buoyancy forces results an increment in the velocity. The inspiration of thermal relaxation time parameter λ_T against temperature profile θ is illustrated in Fig. 8. The temperature profile θ reduces for larger number of thermal relaxation parameter λ_T. Figure 9 manifests the effect of Biot number γ on θ. It is seen that θ increased against larger values of Biot number γ. Physically, the Biot number present the heat transfer coefficient which enhanced the temperature profile. Moreover, the rate of heat transfer is relatively more growing for stretched cylinder as compared to plate. To consequence of sponginess parameter α on θ, Fig. 10 is pictured. It is predicted that θ upsurges for larger values of sponginess parameter α. Fig. 11 is inserted to envision the effect of thermophoresis parameter Nt on thermal field θ of fluid. The thermophoresis phenomenon is based on the collection of nanoparticles which migrated to the cooler surface because of temperature gradient. This fluctuation in temperature due to thermophoresis phenomenon increase

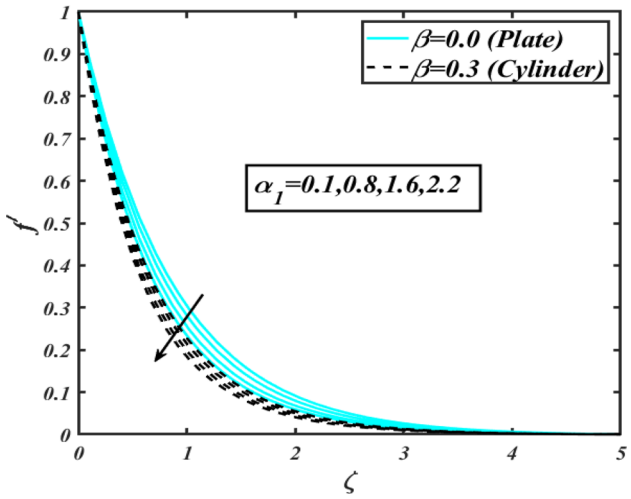

Figure 3. Profile of f' for α_1.

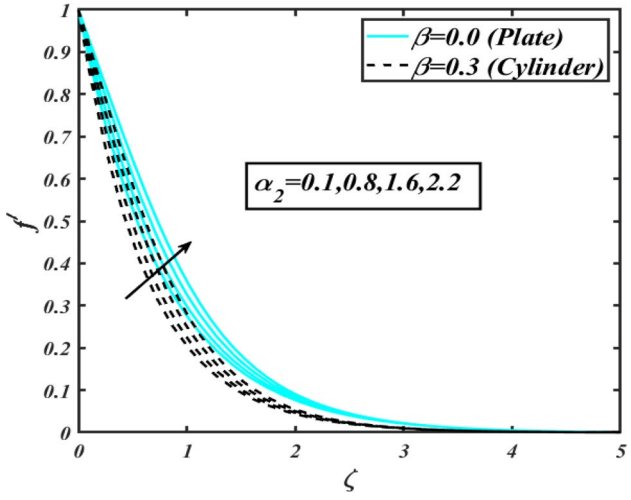

Figure 4. Profile of f' for α_2.

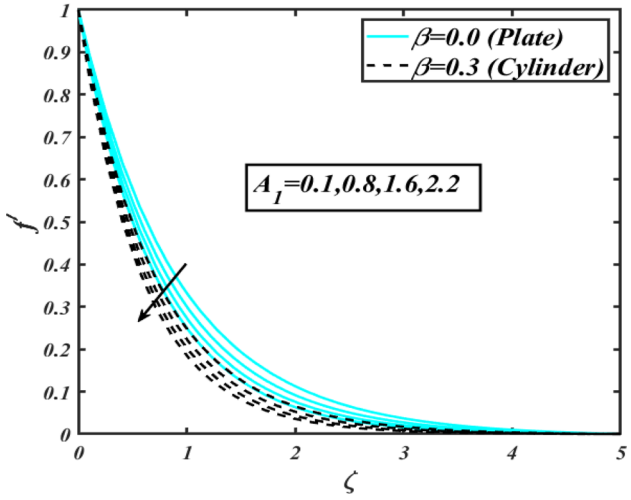

Figure 5. Profile of f' for A_1.

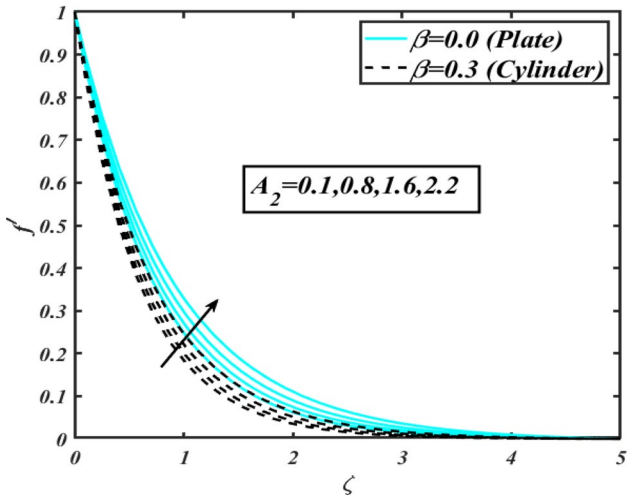

Figure 6. Profile of f' for A_2.

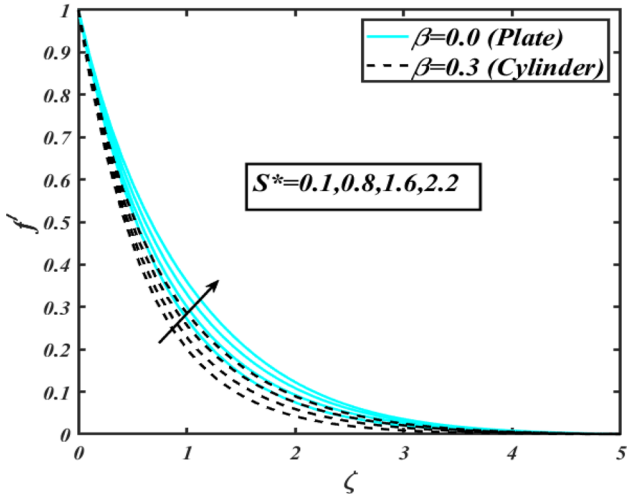

Figure 7. Profile of f' for S^*.

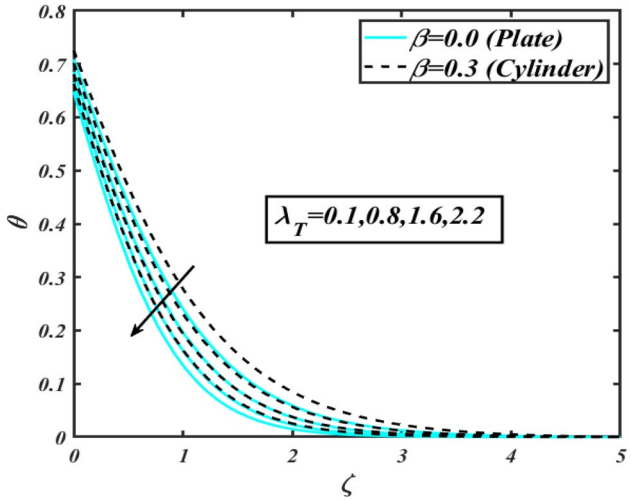

Figure 8. Profile of θ for λ_T.

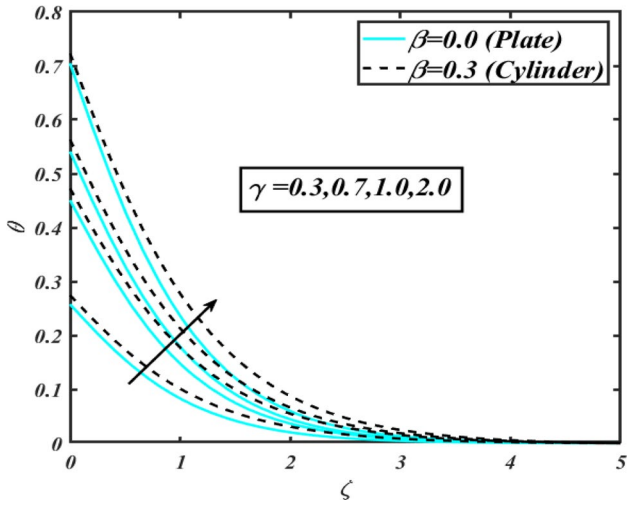

Figure 9. Profile of θ for γ.

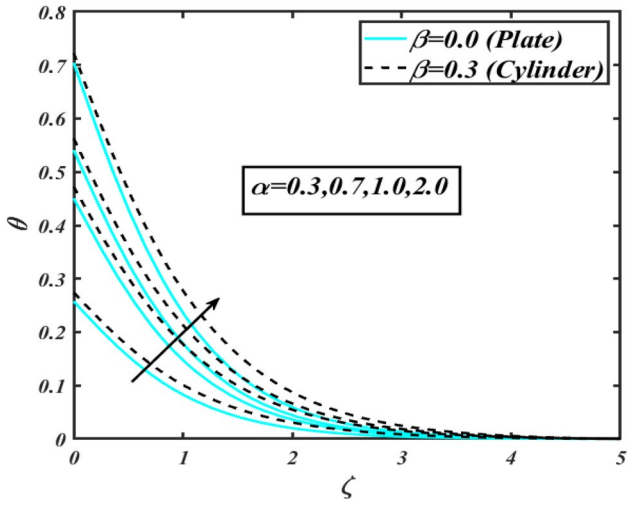

Figure 10. Profile of θ for α.

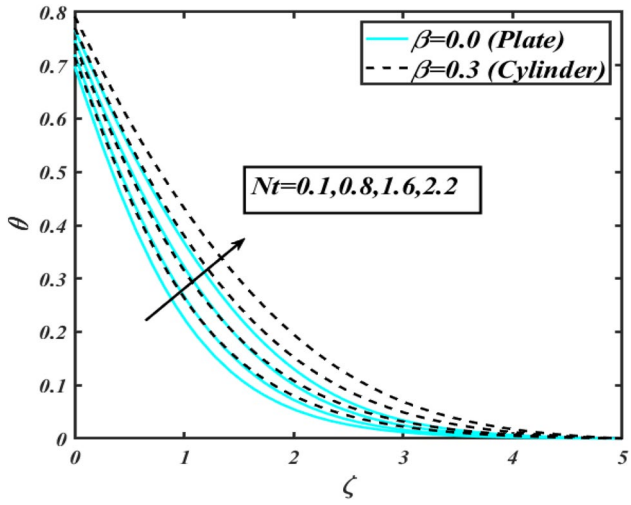

Figure 11. Profile of θ for Nt.

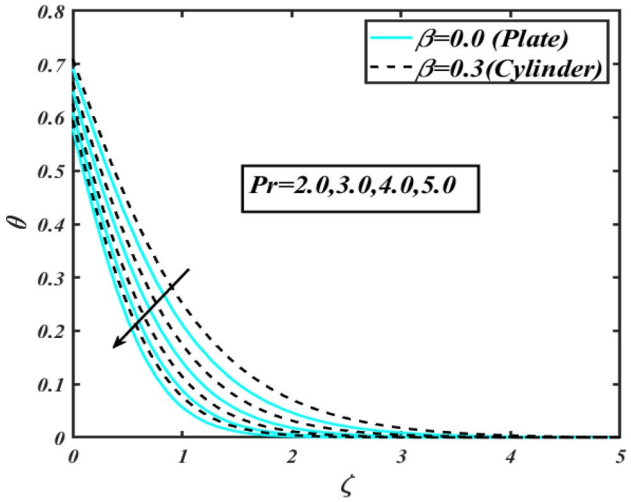

Figure 12. Profile of θ for Pr.

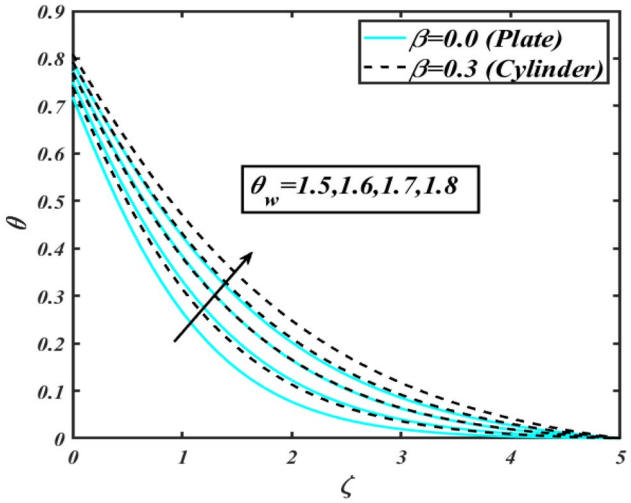

Figure 13. Profile of θ for θ_w.

the temperature profile. Figure 12 reports the inspiration of Prandtl number Pr on θ. The lower temperature changes have been noted due Pr is noted. Physically, the increasing outcomes in Prandtl number declined the thermal diffusivity due to which θ declined. Figure 13 impacted the change in θ due to temperature ratio parameter θ_w. It is analyzed that θ shows an enlarging trend for growing values of temperature ratio parameter θ_w. The effect of solutal relaxation time parameter λ_C against concentration field ϕ is deliberated in Fig. 14. The concentration profile ϕ reduces for λ_C. The features of activation energy parameter E on ϕ is scrutinized in Fig. 15. It is perceived that ϕ enhanced by raising the numbers of activation energy parameter$E$. The activation energy determines the minimum energy supply to start the reaction phenomenon. The presence of activation energy enhanced the concentration change more effectively. The physical aspect of Lewis number Le on ϕ is examined via Fig. 16. The concentration ϕ reduces by augmenting the values of Lewis number Le. Physically, this reduction in concentration is due to low mass diffusivity of nanoparticles associated to the higher values of Lewis number. The physical outcomes of Brownian motion parameter Nb against ϕ of is considered in Fig. 17. The diminishes change in ϕ against larger Nb is noticed. The characteristics of thermophoresis parameter Nt against ϕ is characterized in Fig. 18. The concentration rate ϕ is dwindles with larger thermophoresis parameter Nt. Figure 19 is presented to estimate the variation of bioconvection Lewis number Lb on microorganism field χ for plate ($\beta = 0.0$) and cylinder ($\beta = 0.3$). It is analyzed that microorganism field χ declines with enlarge numbers of Lb. The physical features of Peclet number Pe on χ disclosed in Fig. 20. The lower microorganism rate for higher Pe is observed. The lower microorganism profile with higher Peclet number is owing to low motile diffusivity.

The numerical data is achieved for inspecting the heat transfer rate, mass transfer pattern, motile density and wall shear forces in tables (2, 3, 4, 5). Table 2 suggests that the wall shear rate enhance with Hartmann number while it reduces for mixed convection parameter. The numerical observations are relatively growing for stretched

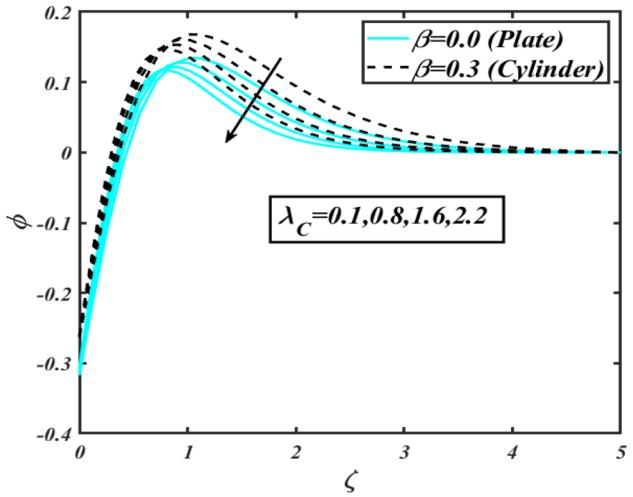

Figure 14. Profile of ϕ for λ_C.

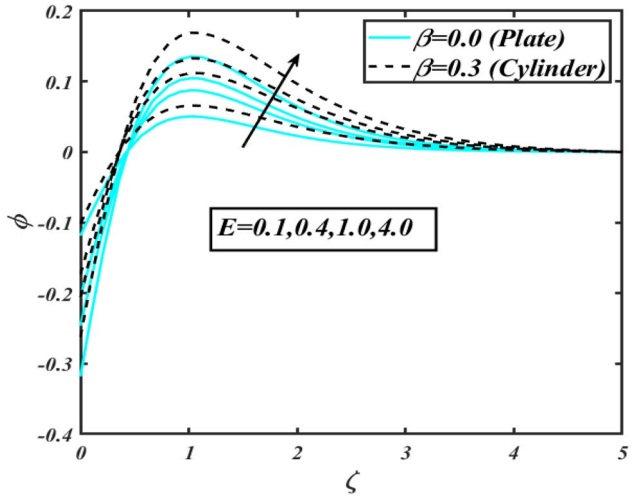

Figure 15. Profile of ϕ for E.

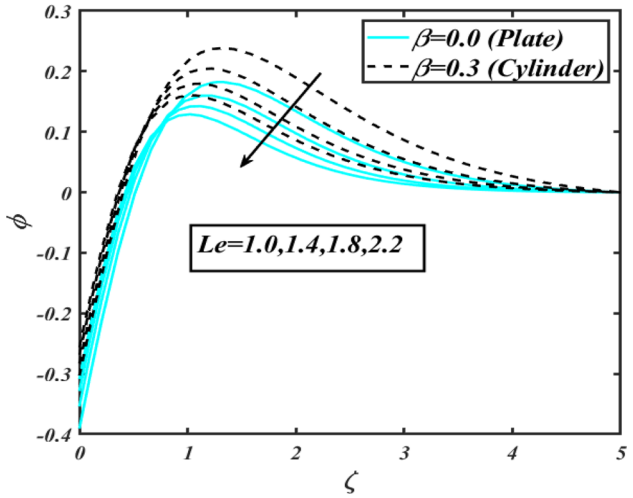

Figure 16. Profile of ϕ for Le.

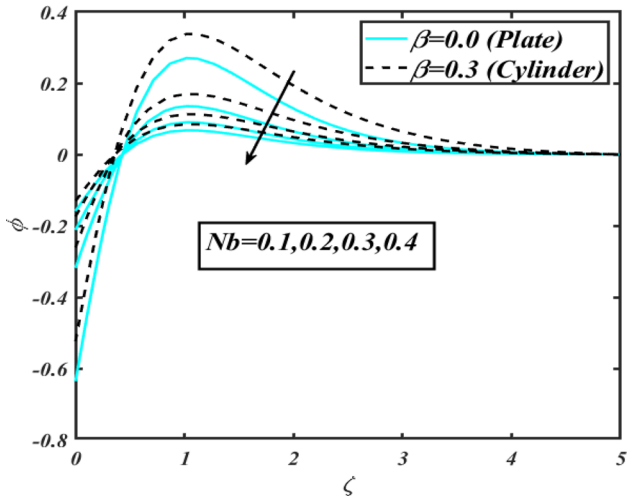

Figure 17. Profile of ϕ for Nb.

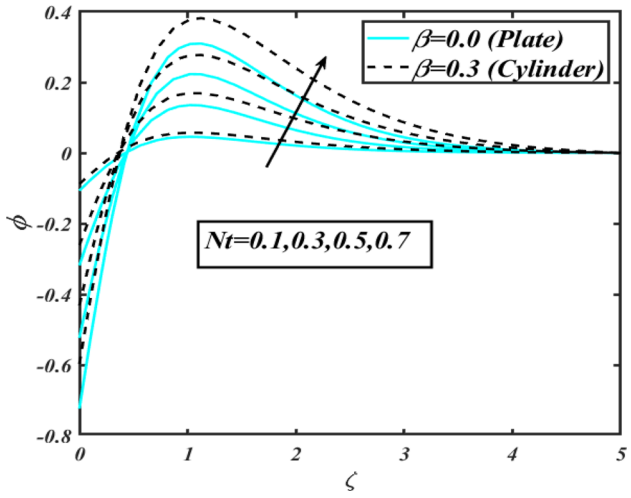

Figure 18. Profile of ϕ for Nt.

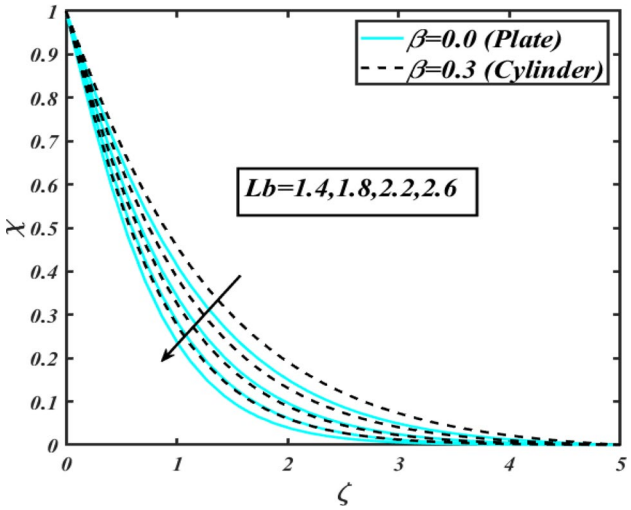

Figure 19. Profile of χ for Lb.

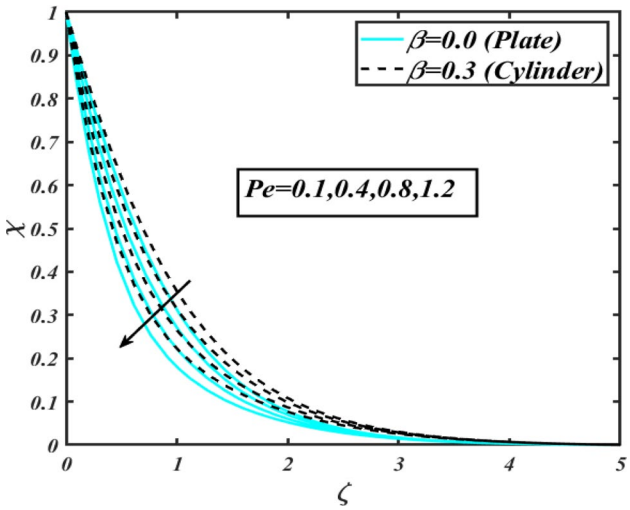

Figure 20. Profile of χ for *Pe*.

Parameters						$-f''(0)$	
M	S^*	A_1	A_2	α_1	α_2	$\beta = 0.0$	$\beta = 0.3$
0.1	0.2	0.1	0.1	0.1	1.0	1.0193	1.3106
0.8						1.3058	1.5981
1.6						1.5705	1.8620
0.5	0.1	0.1	0.1	0.1	1.0	1.1914	1.3598
	1.0					1.1887	1.3469
	2.0					0.1825	1.3376
0.5	0.2	0.2	0.1	0.1	1.0	1.1911	1.4835
		0.8				1.1892	1.4819
		1.6				1.1866	1.4799
0.5	0.2	0.1	0.2	0.1	1.0	1.1922	1.4846
			0.8			1.1969	1.4895
			1.6			1.2030	1.4961
0.5	0.2	0.1	0.1	0.1	1.0	1.1923	1.4787
				0.6		1.1975	1.4867
				1.2		1.2042	1.4939
0.5	0.2	0.1	0.1	0.1	0.1	0.1936	1.4809
					0.6	0.1865	1.4650
					1.2	0.1821	1.4318

Table 2. Outcomes of $-f''(0)$ versus M, S^*, A_1, A_2, α_1 and α_2.

cylinder. The numerical outcomes listed in Table 3 explores the Nusselt number variation when different numerical values are assigned to parameters. The decreasing numerical data is achieved for thermophoresis constant while increasing observations are predicted against thermal relaxation constant. Table 4 notify that the Sherwood number numerical variation is larger for Lewis number and concentration relaxation number. From Table 5, the enhanced numerical data is results against the Peclet number.

Parameters										$-\theta'(0)$	
M	S^*	A_2	A_1	Nt	Nb	Pr	Rd	λ_T	Le	$\beta = 0.0$	$\beta = 0.3$
0.1	0.2	0.1	0.1	0.3	0.2	2	0.8	0.3	2.0	0.6059	0.5734
0.8										0.5726	0.5399
1.6										0.5423	0.5423
0.5	0.1	0.1	0.1	0.3	0.2	2	0.8	0.3	2.0	0.5724	0.5480
	1.6									0.5836	0.5317
	2.0									0.5980	0.5058
0.5	0.2	0.2	0.1	0.3	0.2	2	0.8	0.3	2.0	0.5858	0.5528
		0.8								0.5849	0.5517
		1.6								0.5836	0.5503
0.5	0.2	0.1	0.2	0.3	0.2	2	0.8	0.3	2.0	0.5859	0.5530
			0.8							0.5960	0.5529
			1.6							0.5861	0.5528
0.5	0.2	0.1	0.1	0.1	0.2	2	0.8	0.3	2.0	0.5954	0.5643
				0.6						0.5714	0.5359
				1.2						0.5411	0.5008
0.5	0.2	0.1	0.1	0.3	0.1	2	0.8	0.3	2.0	0.5952	0.5560
					0.6					0.5711	0.5423
					1.2					0.5352	0.5081
0.5	0.2	0.1	0.1	0.3	0.2	1.2	0.8	0.3	2.0	0.4603	0.4295
						2.2				0.6109	0.5782
						3.2				0.7109	0.6802
0.5	0.2	0.1	0.1	0.3	0.2	1.2	0.1	0.3	2.0	0.5767	0.5432
							0.6			0.5841	0.5510
							1.2			0.5885	0.5559
0.5	0.2	0.1	0.1	0.3	0.2	1.2	0.8	0.1	2.0	0.5811	0.5412
								0.6		0.5865	0.5532
								1.2		0.5889	0.5537
0.5	0.2	0.1	0.1	0.3	0.2	1.2	0.8	0.3	1.0	0.5874	0.5545
									2.0	0.5816	0.5487
									3.0	0.5781	0.5453

Table 3. Outcomes of $-f''(0)$ versus M, S^*, A_1, A_2, Nt, Nb, Pr, Rd, λ_T and Le.

Conclusions

The bioconvective thermal determination of Sutterby nanofluid confined via stretched cylinder has been evaluated numerically. The aspect of Darcy resistance for nonlinear radiated flow is also inspected. The numerical outcomes are listed with shooting solver which are further verified to maintain the accuracy. The major results are:

- The declining velocity change for Sutterby nanofluid is observed for Sutterby fluid parameter.
- The increment in velocity change due to Darcy resistance factor is predicted for both stretched cylinder and plate. However, the reducing change in velocity is comparatively progressive for plate.
- The temperature profile for plate and moving cylinder is lower subject to the increasing fluctuation of thermal relaxation constant.
- The stronger heat transmission is observed for sponginess parameter and Biot constant.
- The increasing concertation change of Sutterby nanofluid is noted for activation energy and thermophoresis factor.
- The increasing numerical values of local Nusselt number are predicted for thermal relaxation time constant.

Parameters									$-\phi'(0)$	
M	S^*	A_2	A_1	Nt	Nb	Pr	λ_C	Le	$\beta = 0.0$	$\beta = 0.3$
0.1	0.2	0.1	0.1	0.3	0.2	2	0.3	2.0	0.9089	0.8601
0.8									0.8589	0.8098
1.6									0.8135	0.7663
	0.1	0.1	0.1	0.3	0.2	2	0.3	2.0	0.8642	0.8407
0.5	1.6								0.8763	0.8371
	2.0								0.8860	0.8185
	0.2	0.2	0.1	0.3	0.2	2	0.3	2.0	0.8787	0.8293
0.5		0.8							0.8773	0.8276
		1.6							0.8754	0.8254
	0.2	0.1	0.2	0.3	0.2	2	0.3	2.0	0.8789	0.8295
0.5			0.8						0.8790	0.8294
			1.6						0.8791	0.8293
	0.2	0.1	0.1	0.1	0.2	2	0.3	2.0	0.2977	0.2821
0.5				0.6					1.7141	1.6076
				1.2					3.2467	3.0050
	0.2	0.1	0.1	0.3	0.1	2	0.3	2.0	1.8632	1.6590
0.5					0.6				0.8512	0.2767
					1.2				0.8489	0.1383
	0.2	0.1	0.1	0.3	0.2	1.2	0.3	2.0	0.6904	0.6443
0.5						2.2			0.9163	0.8673
						3.2			1.0663	1.0204
	0.2	0.1	0.1	0.3	0.2	1.2	0.1	2.0	0.8518	0.8421
0.5							0.6		0.8650	0.8322
							1.2		0.8719	0.8272
	0.2	0.1	0.1	0.3	0.2	1.2	0.3	1.0	0.8811	0.5767
0.5								2.0	0.8924	0.5841
								3.0	0.9672	0.5885

Table 4. Outcomes of $-f''(0)$ versus M, S^*, A_1, A_2, Nt, Nb, Pr, λ_C and Le.

Parameters					$-\chi'(0)$	
M	A_1	A_2	Pe	Lb	$\beta = 0.0$	$\beta = 0.3$
0.1	0.1	0.1	0.1	2	0.9749	0.9031
0.8					0.9062	0.8368
1.6					0.8459	0.7813
	0.2	0.1	0.1	2	0.9334	0.8625
0.5	0.8				0.9335	0.8624
	1.6				0.9337	0.8623
	0.1	0.2	0.1	2	0.9330	0.8622
0.5		0.8			0.9371	0.8601
		1.6			0.9286	0.8572
	0.1	0.1	0.2	2	1.0098	0.9285
0.5			1.2		1.8029	1.6069
			2.2		2.6763	2.3147
	0.1	0.1	0.3	2.4	1.0393	0.9666
0.5				2.8	1.1374	1.0636
				3.2	1.2289	1.1545

Table 5. Outcomes of $-f''(0)$ versus M, A_1, A_2, Pe and Lb.

Received: 22 June 2021; Accepted: 18 April 2022
Published online: 07 May 2022

References

1. Choi, S. U. S. Enhancing thermal conductivity of fluids with nanoparticles, development, and applications of non-Newtonian flows. *ASME MD.* **231**, 99–100 (1995).
2. Alharbi, S. O. Influence of wall slip and jump in wall temperature on transport of heat energy in hybrid nanofluid. *J. Therm. Anal. Calorim.* **144**(3), 847–854 (2021).
3. Uddin, M. J., Khan, W. A., Bég, O. A. & Ismail, A. I. M. Non-similar solution of g-jitter induced unsteady magnetohydrodynamic radiative slip flow of nanofluid. *Appl. Sci.* **10**(4), 1420 (2020).
4. Hassan, M., El-Zahar, E. R., Khan, S. U., Rahimi-Gorji, M. & Ahmad, A. Boundary layer flow pattern of heat and mass for homogenous shear thinning hybrid-nanofluid: An experimental data base modeling. *Numer. Methods Part. Differ. Equ.* **37**, 1234–1249 (2021).
5. Tlili, I., Waqas, H., Almaneea, A., Khan, S. U. & Imran, M. Activation energy and second order slip in bioconvection of Oldroyd-B nanofluid over a stretching cylinder: A proposed mathematical model. *Processes* **7**(12), 914 (2019).
6. Khan, S. A., Khan, M. I., Hayat, T. & Alsaedi, A. Darcy-Forchheimer hybrid (MoS2 SiO2) nanofluid flow with entropy generation. *Comput. Methods Programs Biomed.* **185**, 105152 (2020).
7. Haq, F., Saleem, M. & Khan, M. I. Investigation of mixed convection magnetized Casson nanomaterial flow with activation energy and gyrotactic microorganisms. *J. Phys. Commun.* **5**(12), 125001 (2021).
8. Xia, W. F. *et al.* Irreversibility analysis in natural bio-convective flow of Eyring-Powell nanofluid subject to activation energy and gyrotactic microorganisms. *Ain Shams Eng. J.* **12**(4), 4063–4074 (2021).
9. Haq, F., Saleem, M. & Rahman, M. U. Investigation of natural bio-convective flow of Cross nanofluid containing gyrotactic microorganisms subject to activation energy and magnetic field. *Phys. Scr.* **95**, 105219 (2020).
10. Haq, F., Saleem, M., Khan, M. I., Elmasry, Y. & Chinram, R. Entropy generation minimization in bio-convective flow of nanofluid with activation energy and gyrotactic micro-organisms. *AIP Adv.* **11**, 055017 (2021).
11. Hussain, Z., Hayat, T., Alsaedi, A. & Anwar, M. S. Mixed convective flow of CNTs nanofluid subject to varying viscosity and reactions. *Sci. Rep.* **11**, 22838 (2021).
12. Hussain, Z. Heat transfer through temperature dependent viscosity hybrid nanofluid subject to homogeneous-heterogeneous reactions and melting condition: A comparative study. *Phys. Scr.* **96**, 015210 (2021).
13. Hussain, Z., Hussain, A., Anwar, M. S. & Farooq, M. Analysis of Cattaneo-Christov heat flux in Jeffery fluid flow with heat source over a stretching cylinder. *J. Therm. Anal. Calorim.* **147**, 3391–3402 (2022).
14. Madhukesh, J. K. *et al.* Numerical simulation of AA7072-AA7075/water-based hybrid nanofluid flow over a curved stretching sheet with Newtonian heating: A non-Fourier heat flux model approach. *J. Mol. Liq.* **335**, 116103 (2021).
15. Mishra, S. R. *et al.* Control of dusty nanofluid due to the interaction on dust particles in a conducting medium: Numerical investigation. *Alex. Eng. J.* **61**(4), 3341–3349 (2022).
16. Hussain, Z. *et al.* A mathematical model for radiative peristaltic flow of Jeffrey fluid in curved channel with Joule heating and different walls: Shooting technique analysis. *Ain Shams Eng. J.* **13**(5), 101685 (2022).
17. Ahmad, I., Aziz, S., Ali, N. & Khan, S. U. Radiative unsteady hydromagnetic 3D flow model for Jeffrey nanofluid configured by an accelerated surface with chemical reaction. *Heat Transf. Asian Res.* **50**(1), 942–966 (2021).
18. Mir, N. A. *et al.* Analysis of thermally stratified flow of Sutterby nanofluid with zero mass flux condition. *J. Market. Res.* **9**(2), 1631–1639 (2020).
19. Nawaz, M. Role of hybrid nanoparticles in thermal performance of Sutterby fluid, the ethylene glycol. *Phys. A Stat. Mech. Appl.*. **537**, 122447 (2020).
20. Bilal, S., Sohail, M., Naz, R. & Malik, M. Y. Dynamical and optimal procedure to analyze the exhibition of physical attributes imparted by Sutterby magneto-nanofluid in Darcy medium yielded by axially stretched cylinder. *Can. J. Phys.* **98**(1), 1–10 (2020).
21. Sabir, Z. *et al.* A numerical approach for two-dimensional Sutterby fluid flow bounded at a stagnation point with an inclined magnetic field and thermal radiation impacts. *Therm. Sci.* **25**(3), 1975–1987 (2021).
22. Song, Y. Q. *et al.* Bioconvection analysis for Sutterby nanofluid over an axially stretched cylinder with melting heat transfer and variable thermal features: A Marangoni and solutal model. *Alex. Eng. J.* **60**(5), 4663–4675 (2021).
23. Abbasi, A., Khan, M. I., Farooq, W., Khan, S. U. & Amer, H. Electroosmosis optimized thermal model for peristaltic flow of with Sutterby nanoparticles in asymmetric trapped channel. *Eur. Phys. J. Plus* **136**, 1207 (2021).
24. Waqas, H., Khan, S. U., Hassan, M., Bhatti, M. M. & Imran, M. Analysis on the bioconvection flow of modified second-grade nanofluid containing gyrotactic microorganisms and nanoparticles. *J. Mol. Liq.* **291**, 111231 (2019).
25. Aziz, S., Ahmad, I., Khan, S. U. & Ali, N. A three-dimensional bioconvection Williamson nanofluid flow over bidirectional accelerated surface with activation energy and heat generation. *Int. J. Mod. Phys. B* **35**(09), 2150132 (2021).
26. Khan, S. U., Waqas, H., Bhatti, M. M. & Imran, M. Bioconvection in the rheology of magnetized couple stress nanofluid featuring activation Energy and Wu's slip. *J. Non-Equilib. Thermodyn.* **45**(1), 81–95 (2020).
27. Tong, Z. W. *et al.* Nonlinear thermal radiation and activation energy significances in slip flow of bioconvection of Oldroyd-B nanofluid with Cattaneo-Christov theories. *Case Stud. Therm. Eng.* **26**, 101069 (2021).
28. Li, Y. *et al.* A numerical exploration of modified second-grade nanofluid with motile microorganisms, thermal radiation, and Wu's slip. *Symmetry.* **12**(3), 393 (2020).
29. Alwatban, A. M., Khan, S. U., Waqas, H. & Tlili, I. Interaction of Wu's slip features in bioconvection of Eyring Powell nanoparticles with activation energy. *Processes* **7**(11), 859 (2019).
30. Hussain, Z., Hayat, T., Alsaedi, A. & Ullah, I. On MHD convective flow of Williamson fluid with homogeneous-heterogeneous reactions: A comparative study of sheet and cylinder. *Int. Commun. Heat Mass Transfer* **120**, 105060 (2021).
31. Hayat, T., Ayub, S., Alsaedi, A., Tanveer, A. & Ahmad, B. Numerical simulation for peristaltic activity of Sutter by fluid with modified Darcy's law. *Results Phys.* **7**, 762–768 (2017).
32. Fathizadeh, M. *et al.* An effective modification of the homotopy perturbation method for MHD viscous flow over a stretching sheet. *J. King Saud Univ. Sci.* **25**, 107–113 (2013).
33. Fang, T., Zhang, J. & Yao, S. Slip MHD viscous flow over a stretching sheet: Exact solution. *Commun. Nonlinear Sci. Numer. Simul.* **14**, 3731–3737 (2009).

Acknowledgements

The corresponding author Dr. Iskander Tlili would like to thank Deanship of Scientific Research at Majmaah University for supporting this work under the Project Number No. R-2022-131.

Author contributions

All authors contribute equally.

Competing interests
The authors declare no competing interests.

Additional information
Correspondence and requests for materials should be addressed to I.T.

Reprints and permissions information is available at www.nature.com/reprints.

Publisher's note Springer Nature remains neutral with regard to jurisdictional claims in published maps and institutional affiliations.

Open Access This article is licensed under a Creative Commons Attribution 4.0 International License, which permits use, sharing, adaptation, distribution and reproduction in any medium or format, as long as you give appropriate credit to the original author(s) and the source, provide a link to the Creative Commons licence, and indicate if changes were made. The images or other third party material in this article are included in the article's Creative Commons licence, unless indicated otherwise in a credit line to the material. If material is not included in the article's Creative Commons licence and your intended use is not permitted by statutory regulation or exceeds the permitted use, you will need to obtain permission directly from the copyright holder. To view a copy of this licence, visit http://creativecommons.org/licenses/by/4.0/.

© The Author(s) 2022